Evidence of local power deposition and electron heating by a standing electromagnetic wave in electron-cyclotron-resonance plasma

A. Durocher-Jean,[1] L. Stafford,[1] S. Dap,[2,3] K. Makasheva,[2,3] and R. Clergereaux[2,3]
[1]*Département de Physique, Université de Montréal, Montréal, Québec, Canada H3C 3J7*
[2]*Université de Toulouse; UPS, INPT; LAPLACE, 118 route de Narbonne, 31062 Toulouse Cedex 9, France*
[3]*CNRS; LAPLACE; 31062 Toulouse, France*
(Received 23 April 2014; published 11 September 2014)

Microwave plasmas excited at electron-cyclotron resonance were studied in the 0.5–15 mTorr pressure range. In contrast with low-limit pressure conditions where the plasma emission highlights a fairly homogeneous spatial structure, a periodic spatial modulation (period ~6.2 cm) appeared as pressure increased. This feature is ascribed to a local power deposition (related to the electron density) due to the presence of a standing electromagnetic wave created by the feed electromagnetic field (2.45 GHz) in the cavity formed by the reactor walls. Analysis of the electron energy probability function by Langmuir probe and optical emission spectroscopy further revealed the presence of a high-energy tail that showed strong periodic spatial modulation at higher pressure. The spatial evolution of the electron density and of the characteristic temperature of these high-energy electrons coincides with the nodes (maximum) and antinodes (minimum) of the standing wave. These spatially-modulated power deposition and electron heating mechanisms are then discussed.

DOI: 10.1103/PhysRevE.90.033106 PACS number(s): 52.50.Sw, 52.25.Os, 33.50.−j, 52.35.Hr

I. INTRODUCTION

High-density plasmas at electron-cyclotron resonance (ECR) are routinely used in materials processing, for example, for thin films deposition and etching over large-area wafers for microelectronic, optoelectronic, and photonic device applications [1,2]. In an ECR reactor, the plasma is obtained by coupling a static magnetic field with a microwave electromagnetic field. Over the years, various magnetic field configurations have been proposed to tune the plasma characteristics over large-area wafers and/or large volumes. In classical ECR plasmas, high-energy electrons are trapped between two mirror points, producing much higher excitation and ionization efficiencies of the background gas in that region. Electron confinement in the high-magnetic-field regions with the substrate placed in the diffusion region can thus separate the plasma generation and treatment zones, which allows a better control of plasma-surface interactions. Increased charged particle densities and uniformity can be achieved using multipolar magnetic confinement, giving rise to the so-called distributed electron-cyclotron-resonance (DECR) plasmas [3–6]. Since DECR plasmas are based on a combination of antennas and permanent magnets, reactor scaling up to meet specific industrial needs can easily be achieved [1,7–10]. Furthermore, there is a variety of methods for the coupling of the microwave power to the plasma including (i) traveling wave propagation mainly along the magnetic field lines, (ii) propagation mainly across the magnetic field lines, and (iii) standing-wave excitation.

In all cases (traveling or standing wave), the ECR plasma is obtained by achieving the condition of resonance between the electron-cyclotron frequency in the static magnetic field and the frequency of the applied microwave electromagnetic field. Because of the cyclotron resonance, the gyrating electrons rotate in phase with the right-hand circularly polarized wave, seeing a steady electric field over many gyro-orbits. The net result is the production of a sufficient energy gain of the electrons to allow excitation and ionization of the background gas [11]. Such collisionless electron heating allows operating at much lower pressures (typically between 0.075 and 7.5 mTorr) than other plasmas relying only on Ohmic (or collisional) heating. It is well accepted that the electrons heated in the ECR regions are the ones sustaining the plasma [1] such that electron heating is directly attributed to the presence of a static magnetic field. This static magnetic field also improves the discharge efficiency by reducing charged particle losses by diffusion to the walls [12–14].

Other electron heating processes have been reported in these plasmas. In particular, in ECR plasma streams produced in small cavities [15], both left- and right-hand polarized waves can be absorbed in the zones where the plasma density is close to the critical density (the density for which the wave angular frequency ω approaches the electron angular plasma frequency ω_{pe}). Such phenomena are well known in unmagnetized (non-ECR) plasmas sustained by propagating electromagnetic waves (e.g., a traveling surface wave) in the microwave regime [16–18]: The self-consistent interaction between the traveling wave and the plasma is known to produce an overdense discharge (i.e., ω_{pe} higher than ω). A number of interesting phenomena were then reported, including modulation instability and possibilities of soliton formation [19], wave breaking [20], and Landau damping [18,21]. Several studies further pointed out the development of electron plasma resonances near the discharge boundaries where $\omega \cong \omega_{pe}$, resulting from the spatial inhomogeneity of the electron density [18,22–24]. These resonances result in large and sharp peaks of the wave electric field component parallel to the density gradient [18,21–27]. As a result, long-wavelength electromagnetic waves can be resonantly converted into short-wavelength volume plasmons, which can then be absorbed by either collisional or Landau damping. Both experiments and modeling studies have further demonstrated that such resonance can yield enhanced Ohmic heating [18,27] as well as the generation of fast electrons [21,28].

To characterize electron heating in ECR plasmas, extensive fundamental investigations of the electron energy probability function (EEPF) have been reported in the literature. Most authors have shown departure from a Maxwellian distribution, with the EEPF being described by either two [3,25,29] or more [30,31] electron populations, with a high-energy tail attributed to electron heating in ECR regions. Moreover, depending on the experimental conditions, ECR plasmas can develop singular behaviors. For example, Aanesland and Fredrikse [32] reported atypical dependences on pressure of the plasma characteristics with abrupt regime changes. By using a global model, the pressure dependence of the electron density and average electron energy was attributed to the creation of charged particles by electron-impact ionization on ground state atoms balanced by their ambipolar diffusion and recombination on the reactor walls [11,33]. In some cases, hysteresis and instabilities have also been reported with varying pressure [34–36]. Such abnormal behaviors were ascribed to a change in the plasma kinetics either due to a neutral depletion as a result of nonuniform gas heating or to an increase of the number density of metastable atoms, which increases the relative contribution of stepwise ionization processes with respect to electron-impact ionization on ground state atoms.

In this work, Langmuir probe and optical emission spectroscopy are used to study the spatial distribution of electrons along a microwave plasma sustained under ECR conditions. Depending on pressure, the plasma exhibits strong, periodic spatial modulations of the electron density and EEPF that can be attributed to the presence of a standing electromagnetic wave. The precise role of this standing wave on power deposition and electron heating is discussed with respect to phenomena previously reported for plasmas sustained by traveling electromagnetic waves in the microwave regime.

II. EXPERIMENTAL SETUP

Microwave plasma excited at ECR is produced in the reactor illustrated in Fig. 1(a) [3]. The system consists of a stainless steel vacuum chamber with inner dimensions of 110 [x axis on Fig. 1(a)] $\times$ 16 $\times$ 12 cm. The plasma is created by injecting microwaves (2.45 GHz, 150 W) in a 110-cm-long antenna, located parallel to one side of a samarium-cobalt racetrack magnet. The ECR region is located just above the antenna. This specific magnetic field configuration results in two distinct plasma zones: the plasma generation zone near the antenna and the downstream region confined by a second set of permanent magnets. Here, we limited our investigations to the plasma generation zone.

Plasma was generated in a mixture of rare gases (40% Ne, 20% Ar, 20% Kr, and 20% Xe) with pure oxygen. The partial pressure of rare gases and oxygen, controlled by mass flow controllers, were 0.15 and 0.35 mTorr, respectively, yielding a total pressure of 0.5 mTorr (measured with a Baratron gauge). To investigate the influence of pressure on the plasma characteristics, the opening of a butterfly valve located at the entrance of the high-vacuum pumping system was reduced at fixed gas flow rates to reduce the pumping speed and thus to increase the total pressure up to 15 mTorr.

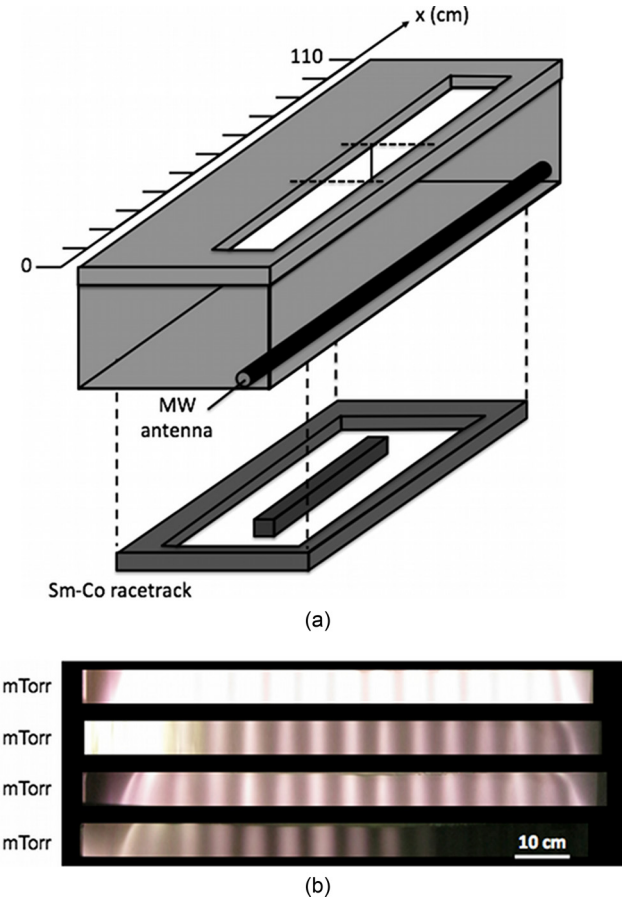

FIG. 1. (Color online) (a) Schematic of the ECR plasma reactor showing the magnets (in the bottom) and the microwave antenna located near the side of the reactor (black line). (b) Optical images of the plasma were taken for different working pressures between 0.5 and 15 mTorr from the top windows schematized in (a). Langmuir probe measurements were performed in the region in the middle of the reactor and the optical emission measurements reported were performed in the region between the two dotted lines.

Langmuir probe measurements were performed using a tungsten cylindrical (200 μm diameter, 1 cm long) probe. For all experiments reported in this paper, the probe was located midway in the plasma chamber (x = 55 cm). It is worth mentioning that with a spatially nonuniform magnetic field varying between 100 and 875 G, the electron Larmor radius for a typical electron energy of 5 eV varies between 85 and 750 μm. Such values being comparable to the probe diameter, magnetic confinement can induce depletion of electrons of low energy and thus a relatively strong distortion of the collected current. To reduce these effects, the probe was placed perpendicularly to the magnetic field line [37]. Moreover, the ion current that must be subtracted from the total current to obtain the corresponding electron population can further hamper probe measurements. This is particularly striking for high-energy electrons, which are associated to an electron current comparable or lower than the ion current. Therefore, as a complement to Langmuir probe measurements, the electron population was also analyzed by optical emission spectroscopy (OES) using a method inspired by the trace-rare-gases optical emission spectroscopy (TRG-OES) technique developed by

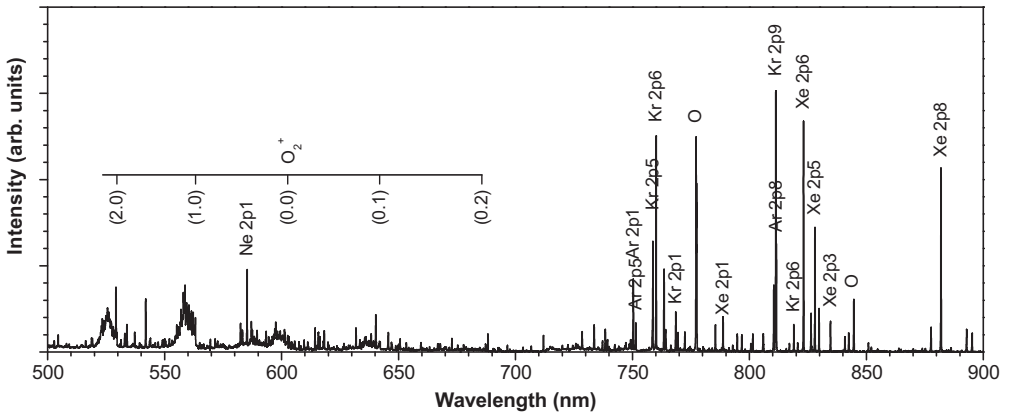

FIG. 2. Typical emission spectrum recorded for plasma in O_2 and rare gases mixture at 1.5 mTorr.

Donnelly [38]. Since the cross sections for electron-impact excitation of the rare gases injected in the gas mixture have quite different energy dependences (in particular, different energy thresholds), the relative emission intensities from Ne, Ar, Kr, and Xe behave quite differently with variations in the EEPF. Moreover, in contrast with the Langmuir probe, OES has the advantage of being nonintrusive and highly sensitive to the high-energy portion of the EEPF, which are unique features to examine electron heating in ECR plasmas. Spatially resolved optical emission spectra were recorded in the plasma generation zone along the antenna using Avantes 3048 Dual-Channel spectrometers: The first one covers the 500–700 nm range while the second one covers the 700–900 nm range, both with a spectral resolution of 0.2 nm. A typical emission spectrum is presented in Fig. 2. In addition to the intense emission from the first negative system of O_2^+ in the 500–700 nm range, very strong emission lines from the $2p$-to-$1s$ (Paschen notation) transitions of the rare gases Ar, Kr, and Xe can also be observed in the 750–900 nm range. For Ne, the emission is dominated by the $2p_1$-to-$1s_1$ transition at 585.2 nm.

III. EXPERIMENTAL RESULTS

Optical images of the plasma along the antenna in the plasma generation zone were taken from the top window schematized in Fig. 1(a). They are reported in Fig. 1(b) for various pressures: 0.5, 1.5, 5, and 15 mTorr. The discharge can be sustained over the entire length of the reactor up to about 5 mTorr. Above this value, the plasma is bright close to the microwave energy input and becomes dimmer along the x direction (at 15 mTorr, axially resolved light emission suggests that the plasma is only ignited in the first 50–60 cm of the reactor). In addition, while a fairly homogeneous spatial structure is observed in low-pressure plasmas (0.5 mTorr), a periodic spatial modulation along the x direction appears as pressure increases.

Optical images were compared to the line-integrated band-head emission intensity of the first negative system of O_2^+ (0,0 at 602.6 nm) and $2p_1$-to-$1s_1$ transition of Ne (585.2 nm) as a function of position along the antenna over the range of pressures for which the plasma is sustained over the entire length of the antenna, i.e., at 0.5, 1.5, and 5 mTorr. The data are shown in Fig. 3. At 0.5 mTorr, the plasma shows very small spatial variation, which is consistent with the nonlocal power deposition characteristics of ECR plasmas. On the other hand, as pressure increases, the emission intensities show periodic spatial modulation comparable to the one displayed in Fig. 1(b).

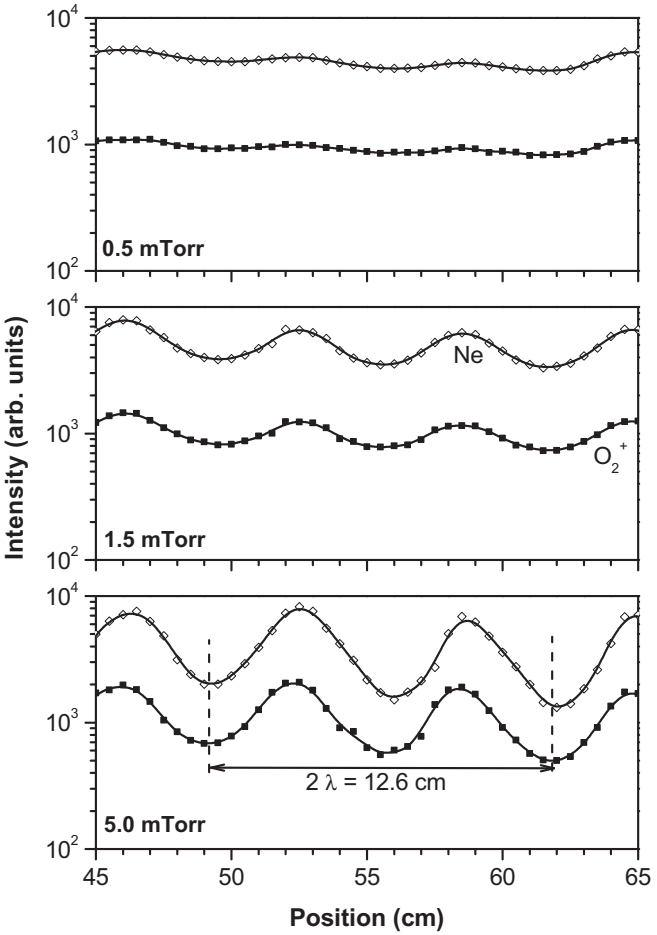

FIG. 3. Ne (585.2 nm) and O_2^+ (602.6 nm) band emission intensities as a function of position along the antenna for 0.5, 1.5, and 5 mTorr in plasmas in a mixture of O_2 and rare gases.

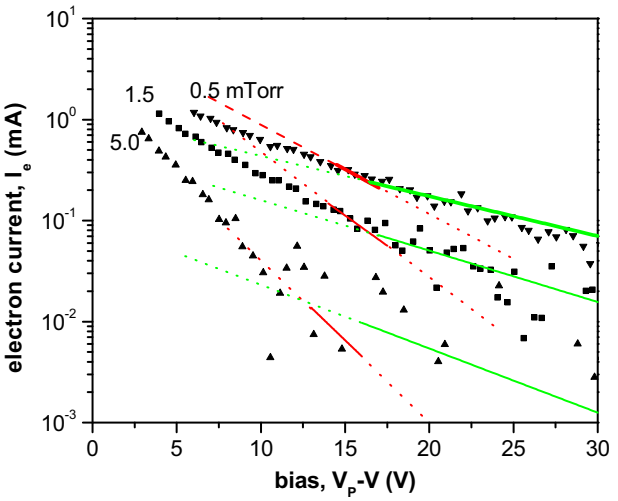

FIG. 4. (Color online) Comparison of the electron current measured by Langmuir probe (symbols) and the segmented electron current constructed using the electron populations determined by OES (lines). The results are shown for plasmas in O_2 and rare gases mixture at 0.5, 1.5, and 5 mTorr.

A number of mechanisms can induce plasma modulations or striations: As commonly observed in the positive column of direct-current discharges, periodic changes in plasma emissions are caused not by the redistribution of a fixed number of electrons (as in plasma waves), but by alternation of regions of predominant production or removal of electrons leading to oscillations of "wavelength" strongly dependent on the operating conditions [39]. However, in our conditions, over the whole range of experimental conditions investigated, the observed modulations were stationary (no propagation) and the wavelength was constant at ~6.2 cm, i.e., half that of the wavelength of the excitation frequency. Based on this result, the spatial modulation displayed in Figs. 1(b) and 3 at higher pressures was ascribed to a "local" power deposition due to the presence of a standing electromagnetic wave at the same frequency as the feed electromagnetic field. This standing wave is created in the cavity formed by the reactor walls (length of about nine times the microwave wavelength in vacuum). Later on we will describe more precisely the role of this standing electromagnetic wave on power deposition and electron heating.

Langmuir probe measurements were performed over the same range of pressures as reported in Fig. 3. The electron currents (after subtraction of the ion current considering a square root function of the bias in the orbital-motion-limited theory) as a function of the probe voltage (using the plasma potential, V_P, as the potential reference found from the zero crossing of the second derivative of the current) are reported in Fig. 4. Over the range of conditions investigated, the average electron energy (or effective electron temperature T_e^{eff}, determined as the slope of the natural logarithm of the electron current) decreases from 7.4 to 5.1 eV as pressure increases from 0.5 to 5 mTorr. Such behavior is consistent with discharge maintenance in which the losses of charged particles by ambipolar diffusion and further recombination on the chamber walls are directly related to the working pressure. In addition, Fig. 4 shows that for all pressures investigated in this work, the electron energy distribution departs from a Maxwellian distribution.

Electron temperatures determined from the Langmuir probe were compared to those obtained by OES. In this context, relative emission intensities from rare gases (Ne, Ar, Xe, Kr) were computed from a collisional-radiative model assuming a Maxwellian electron energy distribution and using the appropriate electron-impact cross sections and branching ratios. The computed emission intensities were then compared with the measured emission intensities (corrected for the optical response of the monochromator and detector) to determine the best fit [38]. From such analysis, three sets of electron temperature can be defined depending on the sets of emission lines used in the fitting operation:

(i) T_e^{tail}, determined using Ar $2p_{1-8}$ and Ne $2p_1$ lines. Ne emission at 585.2 nm is usually very weak in discharges with near-Maxwellian EEPF in gases with ionization potentials lower than the energy of the Ne $2p_1$ levels (18.96 eV above the ground state). However, in this work, this emission could be observed in all conditions (see, for example, Fig. 2), which results from the presence of a high-energy tail in the EEPF [3,25,29,30,40].

(ii) T_e^{high}, found from all Xe, Kr, and Ar lines in which the emitting $2p_x$ levels are mainly populated by electron-impact excitation on ground state Xe, Kr, and Ar atoms. Since these excitations require energies between 9.6 and 13.5 eV, these lines provide an electron temperature that is characteristic of the high-energy part of the EEPF.

(iii) T_e^{low}, found from all Xe, Kr, and Ar lines in which the emitting $2p_x$ levels are mainly populated by electron impact on metastable state Xe, Kr, and Ar atoms. The difference in energy between these metastable states and the emitting $2p_x$ levels being only of a few eVs, T_e^{low} is thus representative of the low-energy portion of the EEPF.

When $T_e^{\text{tail}} = T_e^{\text{high}} = T_e^{\text{low}}$, OES indicates that the EEPF can be assumed Maxwellian, whereas $T_e^{\text{tail}} \neq T_e^{\text{high}} \neq T_e^{\text{low}}$ indicates departures from the Maxwellian energy distribution function.

It is worth mentioning that over the range of experimental conditions investigated in this work, all Ne, Ar, Kr, and Xe levels were populated mainly (>95% as derived from the collisional-radiative model) by electron-impact excitation from the ground state of Ne, Ar, Kr, and Xe atoms. This feature results from the low metastable-to-ground state number density ratios because of the low electron densities $\sim 10^{10}$ cm^{-3} and the high quenching rates of Ar, Kr, and Xe metastables on O_2 [41,42]. As a consequence, the contribution from stepwise excitation of $2p_x$ levels can be ignored such that T_e^{low} cannot be determined. In such cases, relative emission intensities become solely dependent on the electron temperature weighted towards the high-energy portion of the EEPF (T_e^{high} or T_e^{tail} depending on the set of emission lines used in the fitting operation).

In our experiments, over the whole range of pressures investigated, the EEPF departs from a Maxwellian distribution with $T_e^{\text{high}} < T_e^{\text{tail}}$. EEPF based on these two electron populations were constructed using the approach described

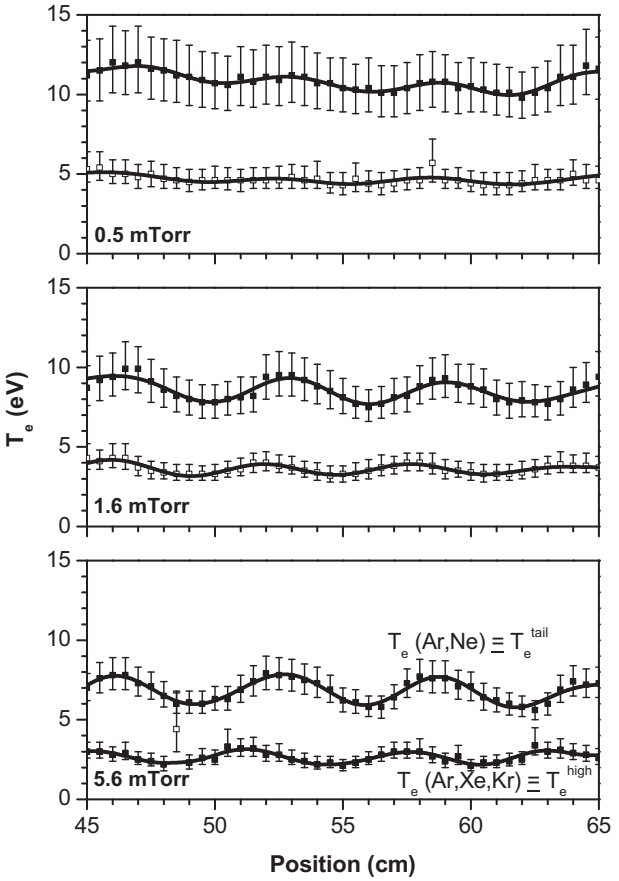

FIG. 5. Electron temperatures determined by OES as a function of position along the antenna (see text for description of T_e^{high} and T_e^{tail}).

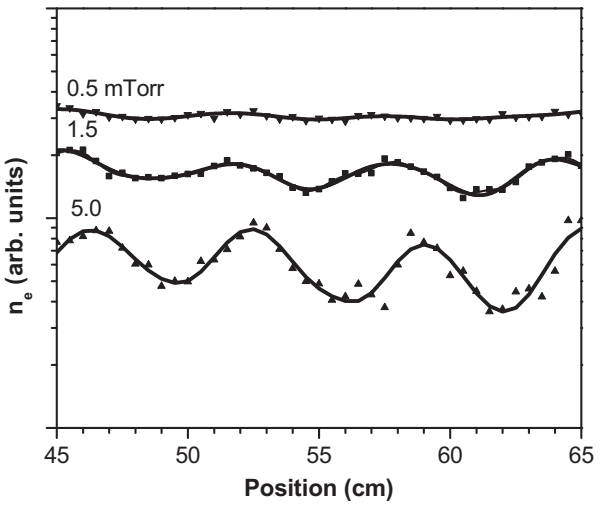

FIG. 6. Ratio of the measured Ne emission intensity at 585.2 nm by the rate coefficient calculated for an electron temperature equal to T_e^{tail} and the operating pressure. Such ratio is linked (in arbitrary units) to the electron density (see text for more details).

in Ref. [43].[1] The results represented as segmented lines in Fig. 4 are compared to those obtained from Langmuir probe measurements. In the high-energy region (>20 eV), despite the high level of noise (due to the small electron current obtained after subtraction of the ion contribution from the total current), an excellent agreement is obtained with both methods for the experiments performed at 0.5 and 1.5 mTorr. Moreover, it allows describing more precisely the tail of the EEPF in the higher-pressure condition (5 mTorr) for which the minimum resolvable current is reached in the Langmuir probe characteristic ($\sim 10^{-3}$ mA).

Spatially resolved OES measurements were performed to study the evolution of the high-energy portion of the EEPF in the presence of the standing electromagnetic wave. The spatial variations of T_e^{high} and T_e^{tail} are shown in Fig. 5 as a function of axial position along the antenna for plasmas obtained at 0.5, 1.5, and 5 mTorr. While T_e^{high} remains much less affected by the standing wave, even at higher pressures, the population of very-high-energy electrons shows strong periodic spatial modulations, with its characteristic temperature T_e^{tail} fluctuating with the nodes (maximum) and antinodes (minimum) of the standing wave.

Following the results displayed in Fig. 5, the spatial modulation of the emission intensities presented in Fig. 3 can in principle be attributed to a spatial variation of the electron density and/or to a change of the EEPF. Given the spatially modulated values of T_e^{tail} presented in Fig. 5, we have estimated the spatial profile of the electron density for the three different pressures using the relative emission intensities of Ne at 585.2 nm. Assuming that the $2p_1$ level of Ne giving rise to this latter emission is populated by electron-impact excitation on ground state Ne atoms and is lost by spontaneous radiation (optically thin medium, the small partial pressure of Ne allowing such assumption), the emission intensity becomes proportional to the ground state number density of Ne, the electron density, and the rate coefficient for electron-impact excitation. The electron density n_e can therefore be estimated from the measured emission intensity at 585.2 nm I (Ne, 585.2 nm), the rate coefficient k calculated for an electron temperature equal to T_e^{tail} and the operating pressure p, proportional to the number density of ground state Ne atoms:

$$n_e \propto \frac{I\,(\text{Ne, } 585.2\text{ nm})}{k\left(T_e^{\text{tail}}\right) p}. \tag{1}$$

The results in arbitrary units are shown in Fig. 6. The strong modulation of the electron density that appears as pressure increases from 0.5 to 5 mTorr indicates that the standing electromagnetic wave influences both power deposition (related to the electron density) and electron heating (related to the electron temperature).

[1]The lower, E_l, and upper, E_h, electron energies used to plot the high-energy segmented line were defined such that 90% of the emission is excited by electrons with energies above E_l and below E_h. These values were computed for $2p_x$ levels of Ar, Kr, and Xe as a function of T_e^{high} using cross sections for electron-impact excitation from the ground state of Ar, Kr, and Xe. For example, for $T_e^{\text{high}} =$ 3.6 eV at 1.5 mTorr, $E_l = 14.0$ eV and $E_h = 17.5$ eV. For the tail, the segmented line is plotted above 18.9 eV.

IV. DISCUSSION

In ECR plasmas, the time-averaged power absorbed per electron is given by [44,45]

$$\Theta_{abs}(x) = \frac{e^2 \nu_e}{4m_e}\left[\frac{1}{\nu_e^2+(\omega-\omega_{ce})^2}+\frac{1}{\nu_e^2+(\omega+\omega_{ce})^2}\right]|E(x)|^2, \quad (2)$$

where $|E(x)|$ is the magnitude of the electric field at the position x, ν_e is the electron-neutral collision frequency for momentum transfer, and ω and ω_{ce} are, respectively, the microwave angular frequency and the electron-cyclotron frequency. At very low pressures, $\nu_e \ll \omega$ such that the power absorbed from the electric field under ECR conditions ($\omega \sim \omega_{ce}$) tends to infinity, independently of the amplitude of the local electric field. On the other hand, as pressure increases, the absorbed power under ECR conditions becomes a function of both the collision frequency and the electric field intensity. As a consequence, in the presence of a standing electromagnetic wave, the inhomogeneous electric field intensity along the microwave antenna can induce nonuniform power deposition along the reactor in the ECR zone and thus yields inhomogeneous light emission patterns in the x direction and electron density, as seen in Figs. 1, 3, and 6.

In addition to the nonuniform power deposition in the ECR zone, the set of experimental data presented above further shows spatial modulation of T_e^{tail} (Fig. 5). As reported by other authors [3,29–31,40], the presence of a high-energy tail in the EEPF of ECR plasmas is attributed to electron heating in nonuniform magnetic field configurations. In the ECR reactor examined in the present study, the magnetic field intensity is homogeneous along the antenna, except very close to the U-turn on the extremities of the racetrack magnet close to the reactor walls. This indicates that spatial modulation of T_e^{tail} cannot be attributed to axial gradients of the magnetic field intensity.

A number of other mechanisms can yield spatially modulated electron heating. Stochastic electron heating due to oscillating plasma sheaths cannot be invoked in microwave discharges since the excursion lengths per oscillating cycle are much smaller than the plasma dimensions. On the other hand, as mentioned above, in spatially inhomogeneous plasmas, electron plasma resonances can develop where ω_{pe} approaches ω. In such resonant conditions, the plasma permittivity tends towards zero, which yields very-high-intensity electric fields in the direction parallel to the density gradient [18,25–27]. Excluding the range close to the electron plasma resonance, the inhomogeneity only weakly modifies the wave propagation characteristics: The dispersion relation can be reasonably well described assuming a homogeneous plasma with a density of charged particles averaged over the cross section [24]. However, such resonance can represent an important mechanism of dissipation of the wave energy (resonant absorption), in addition to Ohmic and/or ECR heating. In unmagnetized low-pressure plasma columns sustained by propagating electromagnetic surface waves (overdense plasma) in which charged particles are essentially lost by ambipolar diffusion and further recombination on the chamber walls, this resonance occurs close to the plasma boundaries (reactor walls and column end, i.e., the position where the transition from the overdense plasma to the underdense plasma takes place). On the other hand, in the ECR reactor under investigation, resonance must occur in the region of maximum power deposition (i.e., at the position where the transition from the underdense plasma to the overdense plasma takes place). As reported in Ref. [46], such resonant condition where $\omega \cong \omega_{pe}$ can be reached in ECR sources near the magnet where power absorption by electrons is maximum [see Eq. (2)].

As discussed in Ref. [24], resonant absorption in spatially inhomogeneous plasmas is due to the linear transformation of electromagnetic waves into electrostatic Langmuir waves (volume plasmons) at the resonant point $\omega \cong \omega_{pe}$. As mentioned above, such absorption can yield to enhanced Ohmic heating [18,27] as well as to the generation of fast electrons [21,28]. While Ohmic heating in the resonance region is related to the collisional damping of the volume plasmons, fast electron generation is related to the noncollisional, Landau-type damping of the volume plasmons, in particular those with large wave numbers, i.e., short plasma waves, which are strongly damped. To play an important role in our conditions, these electrostatic plasma waves would need wavelengths much smaller than those of observed spatial modulations, i.e., ~0.01–0.1 cm. For a wave frequency of 2.45 GHz, this corresponds to phase velocities in the 2–20 $\times$ 10^7 cm s^{-1} range and thus to electron energies between 0.2 and 20 eV. Such group of electrons can therefore be accelerated in the resonance region where resonant wave conversion occurs to fill the tail of the EEPF. In a way similar to the power deposition profile, such collisionless electron heating mechanism is expected to yield spatial modulation of the population of high-energy electrons, in agreement with our experimental data (spatial modulation of T_e^{tail} in Fig. 5).

Despite the highly localized nature of the electron plasma resonance, the observed spatial modulations in the electron temperatures are much less severe than those of the resonant electric field. This is because in the low-pressure plasma investigated in the present work with $\nu_e \ll \omega$ ($\nu_e/\omega \sim 10^{-3} - 10^{-4}$), the local field approximation is inappropriate such that fast electron generation is not confined to the resonance region. Thus, an analysis based on the nonlocal approach was performed. This approach relies on the idea that the electrons are preferentially heated in selective regions of the discharge (due to the strong inhomogeneity of the electromagnetic field) and they are able to move across the discharge with an almost constant energy [18,24,27,47]. The range of validity of the nonlocal approach can be determined from the energy relaxation length $\lambda_e = \lambda_{f.p.}(\nu_e/\nu^*)^{1/2}$, where $\lambda_{f.p.}$ is the electron mean free path and ν^* is the total inelastic collision frequency. λ_e values for the gas mixture investigated in this work were estimated using BOLSIG + [48], with the average electron energy (or effective electron temperature) as input parameter. At 0.5 mTorr ($T_e^{\text{eff}} = 7.4$ eV), λ_e, estimated at about 250 cm, is much greater than the largest dimension of the plasma reactor (x axis of 110 cm). In other words, in such very-low-pressure conditions, the energy gained by the electrons due to the established standing wave is largely distributed all over the plasma and the emission highlights a fairly homogeneous spatial structure. This phenomenon is in good agreement with Lagarde *et al.* [3] where, though they surmised the existence of standing electromagnetic waves

in their ECR plasma reactor, power deposition and electron heating is completely redistributed over the plasma volume. Indeed, as in our case for the condition at 0.5 mTorr, the energy relaxation length of electrons is always much larger than the plasma dimensions and the plasma highlights a homogeneous spatial structure despite the inhomogeneous distribution of the electric field along the microwave antenna.

On the other hand, as pressure increases, the energy relaxation length of electrons becomes smaller than the plasma dimensions such that the inhomogeneous electric field distribution along the antenna affects the spatial distribution of the power deposition [Eq. (2)], and thus the resulting plasma characteristics (electron density and temperature). For example, at 5 mTorr ($T_e^{\text{eff}} = 5.1$ eV), $\lambda_e \cong 8.6$ cm, which is comparable to the wavelength of the standing wave ($\sim$6.2 cm). The previous calculations explain why the spatial modulation of the plasma characteristics becomes more and more visible as pressure increases. It supports the aforementioned mechanism: Electrons can be spatially heated due to the conversion of the standing wave into volume plasmons at the resonant point where the field frequency is equal to the electron plasma frequency and the absorption of these electrostatic oscillations can occur by Landau damping.

V. CONCLUSION

In summary, spatially inhomogeneous power deposition was observed along the antenna of an ECR plasma. This feature was attributed to the presence of a standing electromagnetic wave at the same frequency as the feed electromagnetic field. Such axial distribution of power deposition (related to the electron density) was also associated to a spatial modulation of the high-energy tail of the EEPF; a feature that can be linked to the presence of a plasma resonance in the high-standing-wave electric field regions where the field frequency is equal to the electron plasma frequency. Electron heating in such resonant conditions can be attributed to a wave-particle interaction due to the conversion of long-wavelength electromagnetic waves into short-wavelength volume plasmons at the resonance point.

ACKNOWLEDGMENTS

The authors would like to acknowledge the financial support of (i) the Commission Permanente de Coopération Franco-Québécoise (CPCFQ) through the Samuel de Champlain program, (ii) the Université Paul Sabatier de Toulouse and Université de Montréal through their international outline agreement, (iii) the National Science and Engineering Research Council of Canada (NSERC) through the discovery grant (L.S.) and undergraduate student research award (A.D.), and (iv) the 3PC-working group of the RTRA STAE in France. The authors would also like to thank Dr. Joëlle Margot and Dr. Jacques Pelletier for useful discussions on ECR plasmas.

[1] M. Pichot, A. Durandet, J. Pelletier, Y. Arnal, and L. Vallier, Rev. Sci. Instrum. **59**, 1072 (1988).
[2] S. Zembutsu and T. Sasaki, Appl. Phys. Lett. **48**, 870 (1986).
[3] T. Lagarde, Y. Arnal, A. Lacoste, and J. Pelletier, Plasma Sources Sci. Technol. **10**, 181 (2001).
[4] M. M. Moslehi and S. S. Huang, U.S. Patent No. 4,996,077 A (1991).
[5] M. C. H. Jiang Nan, B. Agius, F. Plais, and D. Pribat, J. Vac. Sci. Technol. **18**, 161 (1998).
[6] S. Point, T. Minea, M.-P. Besland, and A. Granier, Eur. Phys. J. Appl. Phys. **34**, 157 (2006).
[7] T. Lagarde, J. Pelletier, and Y. Arnal, Plasma Sources Sci. Technol. **6**, 53 (1997).
[8] L. Latrasse, A. Lacoste, J. Sirou, and J. Pelletier, Plasma Sources Sci. Technol. **16**, 7 (2007).
[9] D. Hemmers, H. Kempkens, and J. Uhlenbusch, J. Phys. D: Appl. Phys. **34**, 2315 (2001).
[10] H. Amemiya and S. Ishii, Jpn. J. Appl. Phys. **28**, 2289 (1989).
[11] M. A. Lieberman and A. J. Lichtenberg, *Principles of Plasma Discharges and Materials Processing* (John Wiley & Sons Inc., Hoboken, NJ, 2005).
[12] O. A. Popov, S. Y. Shapoval, M. D. Yoder, and A. A. Chumakov, J. Vac. Sci. Technol. A **12**, 300 (1994).
[13] J. Margot, F. Vidal, M. Chaker, T. W. Johnston, A. Aliouchouche, M. Tabbal, S. Delprat, O. Pauna, and D. Benhabib, Plasma Sources Sci. Technol. **10**, 556 (2001).
[14] L. Stafford, J. Margot, F. Vidal, M. Chaker, K. Giroux, J. S. Poirier, A. Quintal-Leonard, and J. Saussac, J. Appl. Phys. **98**, 063301 (2005).
[15] O. A. Popov, J. Vac. Sci. Technol. A **9**, 711 (1991).
[16] I. Odrobina, J. Kudela, and M. Kando, Plasma Sources Sci. Technol. **7**, 238 (1998).
[17] M. Moisan, A. Shivarova, and A. W. Trivelpiece, Plasma Phys. **24**, 1331 (1982).
[18] K. Makasheva and A. Shivarova, Phys. Plasmas **8**, 836 (2001).
[19] D. Grozev, K. Kirov, K. Makasheva, and A. Shivarova, IEEE Trans. Plasma Sci. **25**, 415 (1997).
[20] A. Y. Lee, Y. Nishida, N. C. Luhmann, Jr., S. P. Obenschain, B. Gu, M. Rhodes, J. R. Albritton, and E. A. Williams, Phys. Rev. Lett. **48**, 319 (1982).
[21] Yu. M. Aliev, V. Y. Bychenkov, A. V. Maximov, and H. Schluter, Plasma Sources Sci. Technol. **1**, 126 (1992).
[22] I. Ghanashev, H. Sugai, S. Morita, and N. Toyoda, Plasma Sources Sci. Technol. **8**, 363 (1999).
[23] H. Sugai, I. Ghanashev, and M. Nagatsu, Plasma Sources Sci. Technol. **7**, 192 (1998).
[24] Yu. M. Aliev, H. Schlüter, and A. Shivarova, *Guided-Wave-Produced Plasmas* (Springer-Verlag, Berlin, 2000), p. 75.
[25] T. Terebessy, M. Kando, and J. Kudela, Appl. Phys. Lett. **77**, 2825 (2000).
[26] Yu. M. Aliev, J. Berndt, H. Schluter, and A. Shivarova, Plasma Phys. Controlled Fusion **36**, 937 (1994).
[27] L. L. Alves, S. Letout, and C. Boisse-Laporte, Phys. Rev. E **79**, 016403 (2009).
[28] O. Boudreault, S. Mattei, L. Stafford, J. Margot, M. Moisan, R. Khare, and V. M. Donnelly, Phys. Rev. E **86**, 015402 (2012).
[29] H. J. You, F. W. Meyer, and K. S. Chung, Plasma Sources Sci. Technol. **18**, 015004 (2009).

[30] M. E. Mauel, Phys. Fluids **27**, 2899 (1984).
[31] A. Girard, C. Pernot, G. Melin, and C. Lécot, Phys. Rev. E **62**, 1182 (2000).
[32] A. Aanesland and A. Fredriksen, J. Vac. Sci. Technol. A **19**, 2446 (2001).
[33] W. Han-Ming, D. B. Graves, and R. K. Porteous, Plasma Sources Sci. Technol. **4**, 22 (1995).
[34] E. S. Aydil, J. A. Gregus, and R. A. Gottscho, J. Vac. Sci. Technol. A **11**, 2883 (1993).
[35] F. S. Pool, J. Appl. Phys. **81**, 2839 (1997).
[36] M. A. Jarnyk, J. A. Gregus, E. S. Aydil, and R. A. Gottscho, Appl. Phys. Lett. **62**, 2039 (1993).
[37] F. F. Chen, in *Plasma Diagnostic Techniques*, edited by R. H. Huddlestone and S. L. Leonard (Academic Press, New York, 1965), p. 113.
[38] V. M. Donnelly, J. Phys. D: Appl. Phys. **37**, R217 (2004).
[39] Yu. P. Raizer, *Gas Discharge Physics* (Springer-Verlag, Berlin, 1991).
[40] R. Friedlein, D. Küchler, C. Zippe, G. Zschornack, and H. Tyrroff, Hyperfine Interact. **99**, 225 (1996).
[41] N. C. M. Fuller, M. V. Malyshev, V. M. Donnelly, and P. H. Irving, Plasma Sources Sci. Technol. **9**, 116 (2000).
[42] M. V. Malyshev and V. M. Donnelly, Phys. Rev. E **60**, 6016 (1999).
[43] V. M. Donnelly and M. J. Schabel, J. Appl. Phys. **91**, 6288 (2002).
[44] J. Asmussen, J. Vac. Sci. Technol. A **7**, 883 (1989).
[45] M. Moisan and J. Pelletier, *Physics of Collisional Plasmas: Introduction to High-Frequency Discharges* (Springer, Dordrecht, 2012).
[46] G. J. M. Hagelaar, K. Makasheva, L. Garrigues, and J. P. Boeuf, J. Phys. D: Appl. Phys. **42**, 194019 (2009).
[47] U. Kortshagen, C. Busch, and L. D. Tsendin, Plasma Sources Sci. Technol. **5**, 1 (1996).
[48] G. J. M. Hagelaar and L. C. Pitchford, Plasma Sources Sci. Technol. **14**, 722 (2005).